# Impact of atmospheric rivers on the winter snowpack in the headwaters of Euphrates-Tigris basin

Y. Ezber[1] · D. Bozkurt[2,3,4] · O. L. Sen[1]

## Abstract

Understanding the hydrometeorological impacts of atmospheric rivers (ARs) on mountain snowpack is crucial for water resources management in the snow-fed river basins such as the Euphrates-Tigris (ET). In this study, we investigate the contribution of wintertime (December-January–February) ARs to precipitation and snowpack in the headwater regions of the ET Basin for the period of 1979–2019 using a state-of-the-art AR catalog and ERA5 reanalysis data. The results show that AR days in the headwaters region could be warmer by up to 3 °C and wetter by over 5 mm day$^{-1}$ compared to non-AR days. The contribution of ARs to the total winter precipitation varies from year to year, with a maximum contribution of over 80% in 2010 and an average contribution of 60% over the 40-year period. While snow accumulation on AR days shows spatial variability, the average snow contribution is 27% of the seasonal average, ranging from 12 to 57% for different years. The south-facing parts of the mountain range experience significant snowmelt, with contributions ranging from 15 to 80% for different years. The high total precipitation (60%) and low snowpack (27%) contribution can be attributed to the semi-arid characteristics of the region and the occurrence of rain-on-snow events, where rain falling on existing snow rapidly melts the snowpack. The findings have implications for water resource management and call for continued research to improve our knowledge of ARs and their interactions with the complex terrain of the ET Basin.

## 1 Introduction

An atmospheric river (AR) is defined as "a long, narrow, and transient corridor of strong horizontal water vapor transport that is typically associated with a low-level jet (LLJ) stream ahead of the cold front of an extratropical cyclone" (American Meteorological Society, 2024). 82% of ARs occurring on the western coast of the United States are associated with extratropical cyclones, while only 45% of extratropical cyclones have a paired AR and the distance between

ARs and extratropical cyclones greatly changes (Zhang et al. 2019). The vast amount of poleward moisture transport accounts for almost 90% of the water cycle at midlatitudes (Zhu and Newell 1998). Most of the moisture within ARs occurs in the first few kilometers of the lower troposphere due to neutral moist static stability (Ralph et al. 2005) and is rapidly transported by the LLJ before being lifted by a cold front or the other lifting mechanisms such as orographic lifting (Nayak and Villarini 2017). The combination of high water vapor content with strong horizontal wind results in heavy precipitation on elevated terrain, leading to hazardous flooding events (Ralph et al. 2006; Neiman et al. 2002, 2011; Leung and Qian 2009; Lavers et al. 2011, 2012; Waliser and Guan 2017; De Luca et al. 2017; Ramos et al. 2018; Yang et al. 2018; Ridder et al. 2018; Corringham et al. 2019; Xiong et al. 2019; Lorente-Plazas et al. 2020; Bozkurt et al. 2021). Furthermore, these heavy precipitation events can also trigger landslides (Cordeira et al. 2019) and debris flows (Oakley et al. 2023) in adjacent areas.

AR-induced heavy precipitation can occur particularly when the AR is directed toward topographical barriers (e.g.,

✉ Y. Ezber
ezber@itu.edu.tr

1 Eurasia Institute of Earth Sciences, Istanbul Technical University, Istanbul, Türkiye

2 Departamento de Meteorología, Universidad de Valparaíso, Valparaíso, Chile

3 Center for Climate and Resilience Research (CR)2, Santiago, Chile

4 Center for Oceanographic Research COPAS COASTAL, Universidad de Concepción, Concepción, Chile

Neiman et al. 2002; Ralph et al. 2004; Junker et al. 2008). ARs that are more perpendicular to the topographic barriers result in higher water vapor convergence in the lower troposphere, leading to substantial precipitation (Hecht and Cordeira 2017). The orographic precipitation decreases water vapor transport as the AR penetrates further inland. However, lower or less continuous topography allows further inland penetration of AR-induced precipitation (Rutz et al. 2014).

The hydrometeorological effects of ARs on their target regions can be beneficial or destructive as reflected in the AR scale developed by Ralph et al (2019). On the positive side, ARs bring beneficial rain and snow, which serve as a crucial source of fresh water (Guan et al. 2010, 2013; Dettinger et al. 2011; Rutz and Steenburgh 2012; Lavers and Villarini 2015; Viale et al. 2018; Saavedra et al. 2020). Conversely, ARs can also cause extreme precipitation and/or rapid snowmelt, resulting in hazardous floods due to factors such as rain-on-snow and warm air advection (Ralph et al. 2006; Neiman et al. 2008, 2011; Warner et al. 2012; Kim et al. 2013; Rössler et al. 2014; Guan et al. 2016; Waliser and Guan 2017; Dezfuli 2020; Bozkurt et al. 2021).

ARs primarily impact coastal regions located near vast ocean basins, such as the west coast of the US, Europe, and South America. However, ARs also have the potential to impact regions far inland from their point of origin. Some Atlantic ARs can even reach locations such as Anatolia and the Middle East, which are significantly distant from their initial landfall points (Dezfuli 2020; Bozkurt et al. 2021). Perhaps because of the fact that the magnitude of ARs and their destructive impacts in these regions are not as severe as in other well-known AR regions, they have received less scientific attention (Payne et al. 2020; Dezfuli 2020; Bozkurt et al. 2021).

Euphrates-Tigris (ET) Basin in the Middle East, mostly characterized by arid and semi-arid climates, is influenced by overland ARs. The water scarcity in this basin is mitigated by the Euphrates-Tigris rivers, which are primarily fed by the snowmelt runoff from the Near East's Highlands including the Taurus and Zagros Mountains, often referred to as the water towers of the region. Hence changes in snowpack in the headwaters of these rivers affect the downstream agriculture and domestic freshwater use (Yilmaz et al. 2019). The west–east and southeast-northwest orientations of the Taurus and Zagros mountains ranges act as effective topographic barriers, enhancing windward precipitation from incoming moisture-laden air masses. The main sources of the high amount of annual precipitation during the wet season in the Middle East, including Anatolian Peninsula, are the midlatitude cyclones crossing over the Mediterranean basin, which primarily originate from the Atlantic Ocean (Bozkurt and Sen 2011; Lolis and Türkeş 2016; Batibeniz

et al. 2020), and the cooling of the westerly moist air mass due to topographic lifting (Bozkurt and Sen 2011). The moisture distribution exhibits a west–east gradient across the Mediterranean, with the western part receiving moisture advection from the North Atlantic and the eastern part influenced by the Mediterranean Sea and local moisture recycling (Batibeniz et al. 2020). Additionally, the Red Sea and the tropical Atlantic off the coast of Africa can be critical moisture sources for ARs impacting the Middle East and North Africa (MENA) region and its highlands (Dezfuli 2020; Bozkurt et al. 2021; Francis et al 2022). Studies have also shown that extreme precipitation events over the dry deserts of the Middle East are associated with the intrusion of a mid-latitude upper-level trough, known as the Mediterranean trough, into the subtropics, and the deepening and northward amplification of the surface low pressure over the Red Sea region (de Vries et al. 2018). Furthermore, the presence of a Mediterranean trough and high pressure over the eastern margins of the Arabian Peninsula at the upper atmospheric level trigger the formation of a long, narrow path for warm-moist tropical air transport mostly in the form of an AR. The strength of this trough-ridge system can influence the transport of moist air masses further inland with strong upper-level jets, leading to extreme precipitation events (Bozkurt et al. 2019; Sen et al. 2019; Dezfuli 2020). Additionally, poleward warm air advection can cause floods in this region due to the rapid snow melting during the snowmelt (early spring) season (Bozkurt et al. 2021).

Even though the number of AR-related studies has increased recently for the Euro-Mediterranean-MENA region, these studies mostly exhibit the impacts of hazardous AR-induced floods (Akbary et al. 2019; Dezfuli 2020; Bozkurt et al. 2021; Esfandiari and Lashkari 2021; Sadeghi et al. 2021). Besides, it is also essential to investigate the AR's contribution to the snowpack in the upstream mountainous watersheds. The wintertime snowpack in the highlands is a significant water reservoir, and the snowmelt runoff is the main water resource for all riparian countries in the ET Basin. The main objective of this study is, therefore, to investigate the impacts of ARs on the snowpack in the basin's headwaters in winter, and whether the ARs induce increases in snow accumulation or depletion (due to the potential rain-on-snow effect).

This paper is organized as follows: Section 2 presents the data used and methodology. In Section 3, the results are shown, analyzing wintertime integrated water vapor transport (IVT) pattern and the thermodynamic and dynamic structure of winter ARs over the region. It also focuses on interannual changes in the hydrometeorological variables in the headwater region of the ET Basin, providing an example of an influential winter AR. The conclusions are provided in Section 4.

## 2 Data and methods

This study used the new version of the global AR database released by Guan and Waliser (2019). This updated version of the Tracking Atmospheric Rivers Globally as Elongated Targets (tARget) algorithm (Guan and Waliser 2015; Guan et al. 2018) includes a refined method for identifying the AR axis and adds the capability to track ARs from genesis to termination around the globe. This enhancement specifically facilitates the detection of ARs characterized by climatologically low water vapor transport that travels far inland, which is relevant to the area where this study was conducted. The AR database of Guan and Waliser (2019) was generated for the period of 1979–2019 using IVT calculations from global specific humidity and wind components at 17 pressure levels with a 1.5°x1.5° horizontal resolution and a 6-hourly time resolution of the ERA-Interim reanalysis dataset. The AR detection method, as adopted by Guan and Waliser (2015), provides outputs that include the axis, shape, landfall location, basic statics of frequency, duration, maximum IVT, and event-total IVT AR metrics. More detail about the technique can be found in Guan et al. (2018) and Guan and Waliser (2019). Our approach to studying ARs is based on the criterion that at least one timestep of the dataset is covered by the AR shape boundaries over the area of interest (black dashed box in Fig. 1). In calculating the AR frequency, we applied the method used by Bozkurt et al. (2021) for the same region. This method involves counting the AR shape boundaries detected for 6-h timesteps in each grid cell and dividing it by the total number of 6-h timesteps for the respective period. We define an "AR-day" as a day in which at least one of the four reanalysis times falls within the detected AR shape boundaries over the specified region in Fig. 1. Considerable thought was given to defining the AR-detection region to ensure no potential AR impacts were overlooked from any direction within the ET Basin. Therefore, as depicted in Fig. 1, our focus was on the highlands of the Near East. Yet, since our research centers on the AR's effects on water resources in the ET Basin,
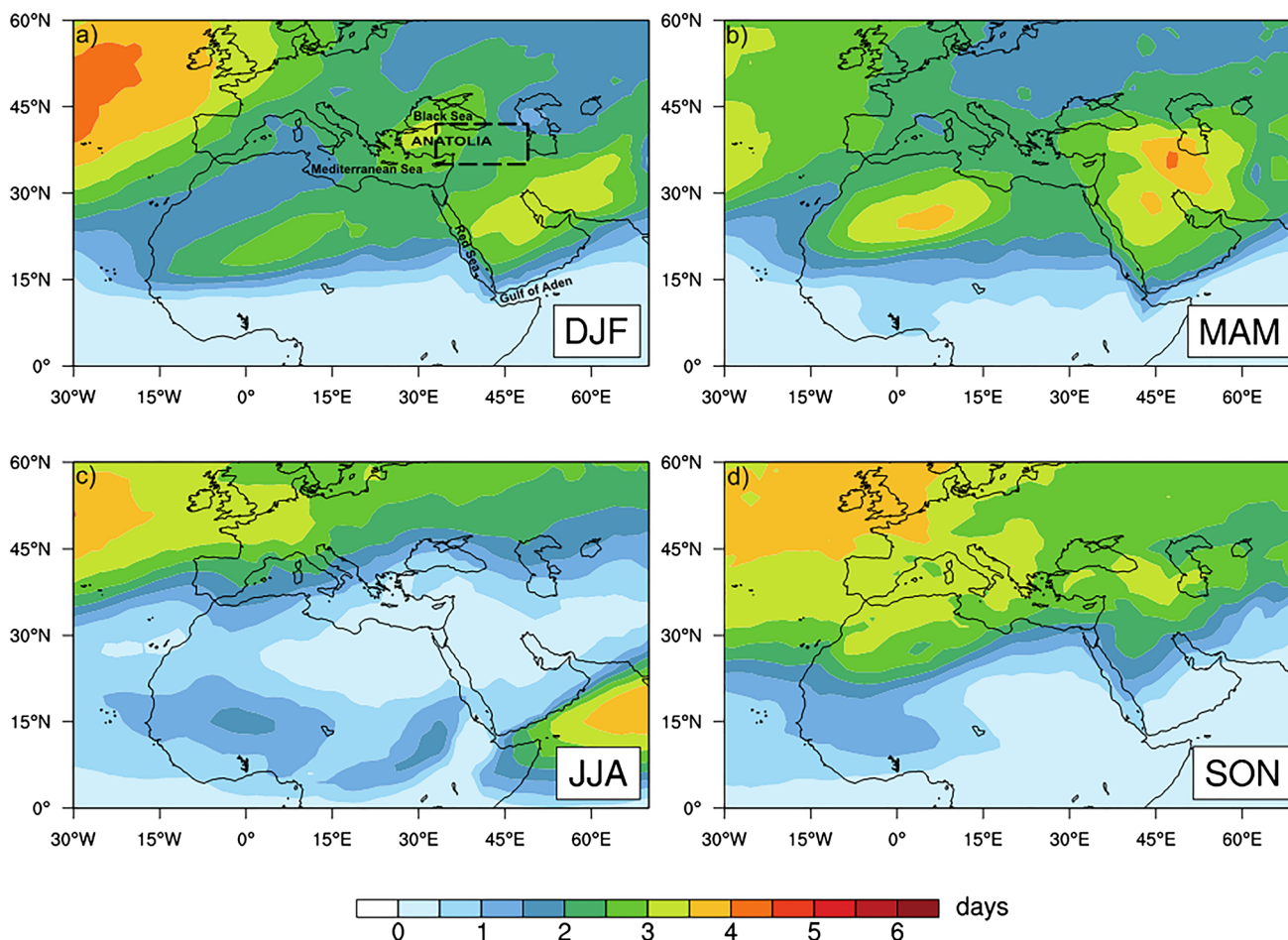


**Fig. 1** AR frequency (days per season) of each season between 1979 and 2019 for the dashed box

we prioritized the headwater region in our impact analysis. We focused on the winter season, which includes the months of December, January, and February (DJF).

For evaluating the AR impacts on the region, we used daily air temperature at 2-m, total precipitation, snow water equivalent (SWE), snowmelt, radiation budget components (net longwave and shortwave radiation, downward shortwave and longwave radiation) data with a horizontal resolution of 0.25°x0.25° from the hourly ERA5 data from ECMWF (Hersbach et al. 2023). In addition to surface data, we used geopotential height at 500 hPa and wind components at 200 hPa to investigate the synoptic scale features on AR days.

The daily changes of hydro-climatological variables (total precipitation, SWE, snowmelt) were calculated using the approach by Guan et al. (2010) and Saavedra et al. (2020). We used a one-day time window that included the day before and the day after each AR event. The daily accumulation was calculated by summing the differences in variables before and after the AR event, and only positive values were considered for the AR contribution. We also calculated changes in snowmelt by applying the same approach to define the AR effects on snowmelt. The Student-t test was applied to determine the significance of IVT and air temperature anomalies on AR days.

## 3 Results

### 3.1 Seasonal AR frequency and wintertime IVT pattern over the euro-mediterranean region

Figure 1 shows the seasonal mean number of days per year with AR conditions (i.e., at least one 6-h AR step) for the 1979–2019 period, where the AR intersects with the dashed box in the figure. The frequency of ARs is relatively high over the North Atlantic (about 4 days) and low in subtropical regions (around 2 days depending on the season). In eastern Anatolia, where the main headwaters are located, AR conditions occur for 2–4 days during winter, fall, and spring, but are rare in summer. The seasonal importance of ARs varies between the west and east of the box, which covers the ET basin, a vital water resource for Mesopotamia. ARs are most frequent during the transition seasons of fall and spring, and a high AR frequency during the spring melting season is crucial for the region's freshwater resources (Bozkurt et al. 2021). However, AR occurrence in winter is also important since it can affect the snowpack over rough terrain.

Batibeniz et al. (2020) demonstrated that the eastern Mediterranean serves as the primary moisture source for the precipitation pattern in its surrounding regions during spring and summer. Figure 2 reveals that this moisture source is also essential in winter, as indicated by relatively large daily mean composites of IVT values (120–180 kg m$^{-1}$ s$^{-1}$) on



**Fig. 2** Composite DJF IVT and IVT vectors (zonal and meridional components) on AR days intersecting with the dashed box for the period 1979–2019
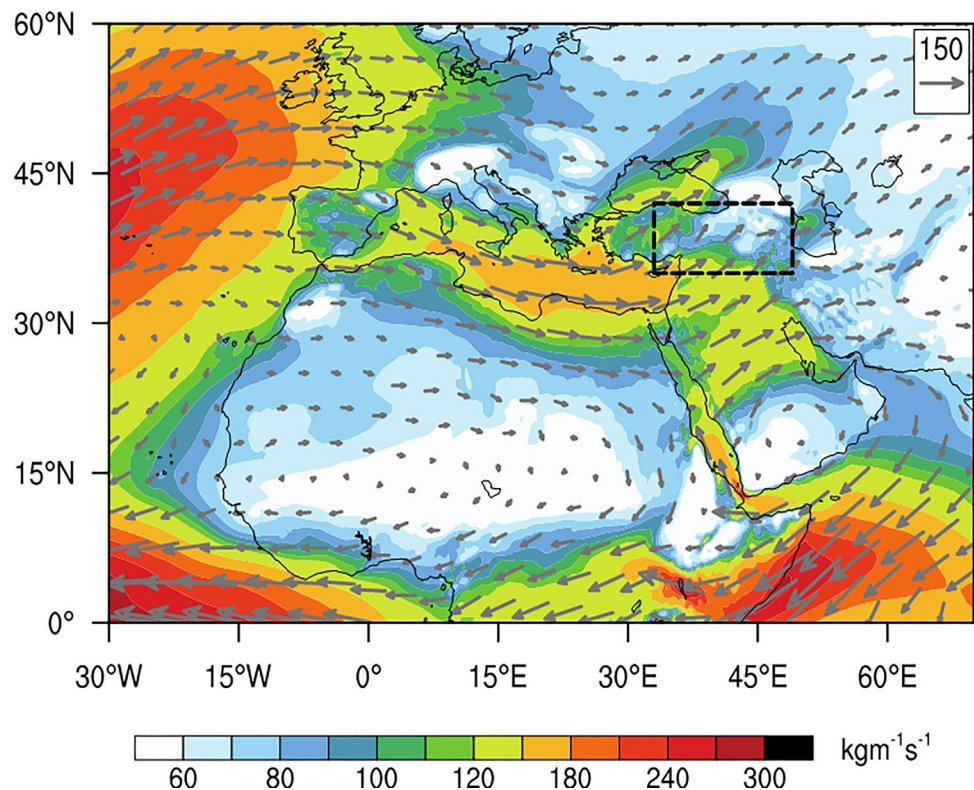
"AR days". The pattern of IVT composites in DJF extends towards the western Mediterranean and the Black Sea. In addition, the AR-affected region is constrained along the coast of northern Africa due to the anticyclone over northern Africa and a diagonal pattern of the Arabian anticyclone that extends between the Red Sea and the Gulf of Aden. IVT values range from 60 to 110 kg m$^{-1}$ s$^{-1}$ over eastern Anatolia (dashed line box). The major features of the IVT patterns are very similar to the findings of Bozkurt et al. (2021) for early spring, except for the diagonal location of the Arabian anticyclone.

### 3.2 Dynamic and thermodynamic background on winter AR days

AR conditions are associated with two ridges over the Atlantic and the Middle East and Caspian Sea Basin, with a trough located over the Mediterranean in between. These large-scale features were also identified by Bozkurt et al (2021) for their study period in March and April. However, for DJF, the locations of these features are more westward. A strong anticyclone dominates over the south of the domain from east-southeast of Türkiye, Middle East to the Caspian Sea, and the broader eastern Mediterranean trough deepens under winter AR conditions with respect to climatology (Fig. 3a). The subtropical jet (200 hPa upper-level winds) is particularly strong over central North Africa, with speeds exceeding 60 ms$^{-1}$ on winter AR days (Fig. SP1a). The jet stream under AR conditions, compared to climatology, strengthens over the entire Mediterranean Basin but weakens over the Middle East due to the presence of high pressure (Fig. SP1b). The

composite daily mean IVT anomalies on winter "AR days" in the Eastern Mediterranean and the Middle East range from $+30$–$60$ kg m$^{-1}$ s$^{-1}$ (statistically significant at 95% confidence level). The IVT in the Levant Basin also exhibits significant anomalies exceeding $+60$ kg m$^{-1}$ s$^{-1}$. Surface air temperature at 2 m indicates a dipole-like anomaly pattern between Europe and the Middle East including Türkiye. The climatological 0 °C contour (green line in Fig. 3b) aligns with the borders of mountain ranges such as the Taurus and the eastern Black Sea Mountains in Anatolia. Significant warmer temperature anomalies over $+3$ °C appear over eastern Anatolia, northeastern Africa, and the Caspian Sea Basin. Moreover, the entire ET Basin experiences significant temperature anomalies (reaching up to $+3$ °C at headwaters) on AR days, which is important considering the changing winter snowpack characteristics in the region that we focus on in the following sections. ARs formed under favorable synoptic conditions also induce changes in hydrometeorological variables in the region.

### 3.3 Hydrometeorological changes on winter AR days

Figures 4a and b show the anomalies in total precipitation and SWE on winter AR days compared to climatology. Following the significant increases in IVT, total precipitation increases in the eastern Mediterranean – Black Sea region (Fig. 4a). The increase is particularly prominent along the Taurus Mountains (above $+3.5$ mm day$^{-1}$) and Zagros Mountains (above $+5$ mm day$^{-1}$). However, despite the precipitation increase, Fig. 4b indicates a decrease in
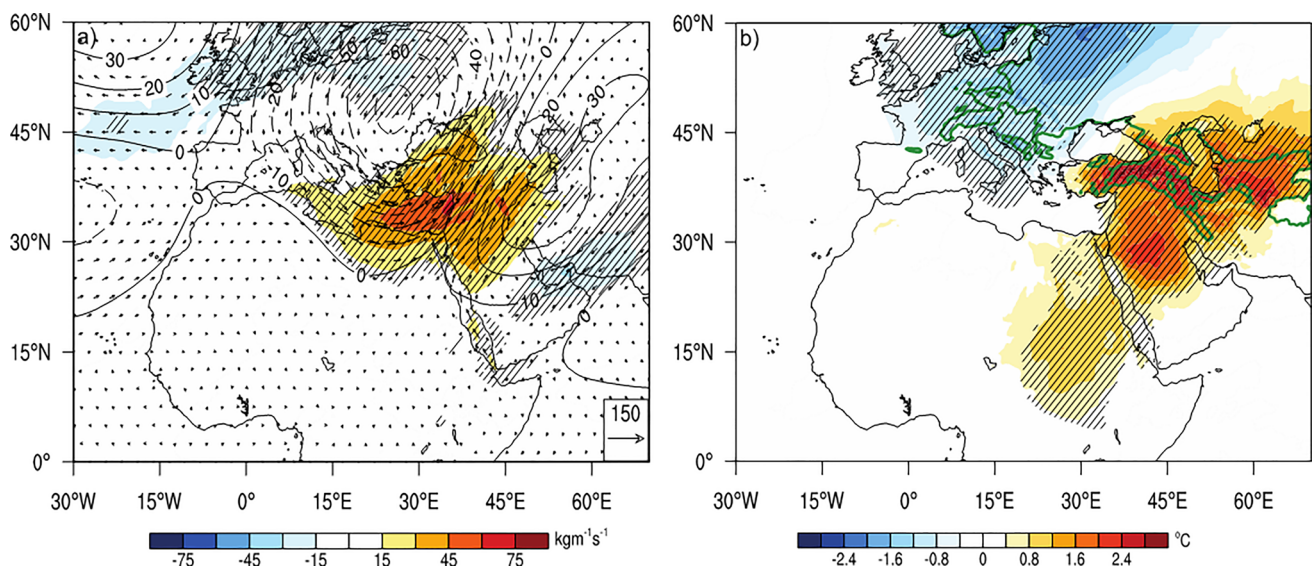


**Fig. 3** **a** Anomalies of IVT (shaded) and IVT vectors (zonal and meridional components), and geopotential height at 500 hPa (contour) on AR days for winter. **b** same as (**a**) but for air temperature at 2 m (shaded), and climatology of 0 °C (green contour). Strips show a 95% significance for IVT and 2-m temperature based on the Student-t test
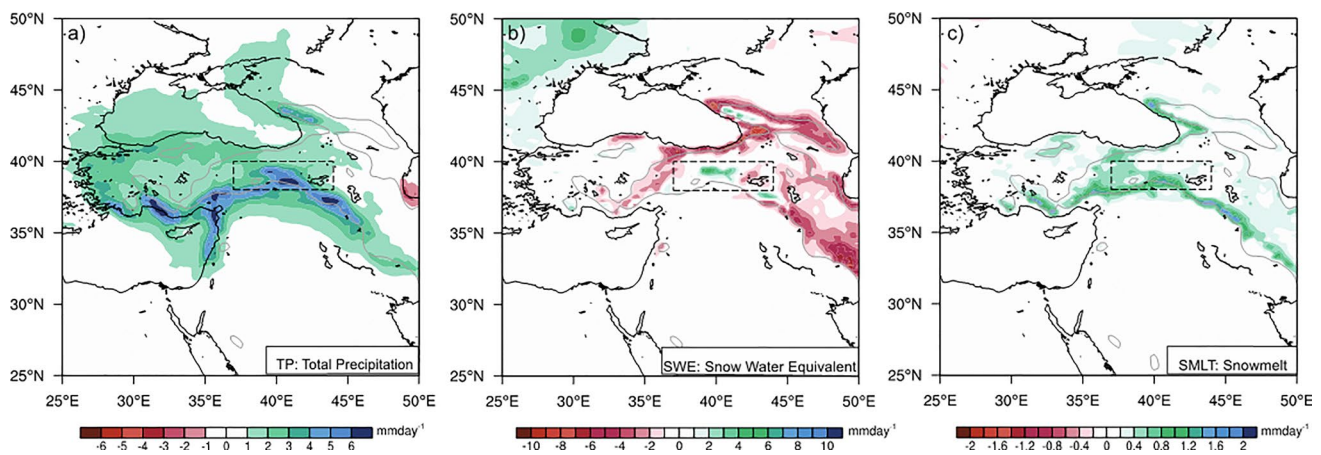
**Fig. 4** Anomalies of AR days from the 1979–2019 DJF climatology for total precipitation (TP) (**a**), snow water equivalent (SWE) (**b**), and snowmelt (SMLT) (**c**). The dashed box demonstrates roughly where the headwaters of the Euphrates and Tigris Basin is located. Gray solid contour shows 1200 m elevation

SWE across most of the region, indicating that precipitation occurs mostly in the form of rain. This is supported by the increased snowmelt below 1200 m elevation on these days (Fig. 4c). Although SWE generally exhibits a declining characteristic, some regions in the eastern Anatolia and Zagros Mountains including the headwaters of the ET Basin experience an increase in SWE (Fig. 4b). On AR days, snowmelt reaches approximately 1 mm day$^{-1}$ along the borders of the high mountain ranges in both the northern and southern parts of the region and around 0.4 mm day$^{-1}$ in eastern Anatolia (Fig. 4c). Similar behavior is observed along the borders of the Taurus and Zagros Mountains, as well as in the upper parts of the headwater region where elevation is below 1700 m.

Figure 4 presents the deviation of variables from the climatology on AR days. However, changes occurring one day before and after the AR events are also associated with the AR events, emphasizing the importance of accounting for lead/lag time responses between AR events and hydrometeorological variables. In this part of the study, we particularly focus on SWE changes to assess the variations in snow accumulation intensity on AR days using a one-day window. Nevertheless, we also examine other surface variables associated with SWE accumulation, such as temperature, total precipitation, and snowmelt.

Figures 5a and b indicate that the average temperature is above 0 °C in the region, except over the high mountainous region, on both AR days and climatology. The temperature pattern shows a distinct warming pattern, which is consistent with the temperature deviation shown in Fig. 3b on AR days. Total precipitation is mostly high along coastal regions, with greater amounts occurring in the high mountain ranges in northern and southern Anatolia and the Zagros Mountains on AR days. Total precipitation accumulation (ΔTP) within

the one-day window over the Anatolian peninsula ranges from 50 mm in inland regions to over 200 mm in the coastal region on winter AR days (Fig. 5c). The climatology of winter total precipitation exceeds 375 mm in the west and northeast coasts of Anatolian Peninsula, while high mountain ranges such as the Taurus, eastern Black Sea, and the Zagros Mountains exhibit a high 40-year climatological winter total TP of 300 mm. Total precipitation for all-day climatology averages around 230 mm in the headwater region of the ET Basin (dashed box in Fig. 5d). On AR days, the accumulation of ΔTP in the headwater region is around 140 mm, contributing around 61% of the all-day climatology of total precipitation. The climatology of winter SWE in the headwater region is approximately 185 mm (Fig. 5f). Snow accumulation (ΔSWE) is more pronounced in the Taurus and the Zagros Mountains on AR days (Fig. 5e). The ET headwater region has a ΔSWE of 62 mm under winter AR conditions, contributing 33% to the all-day climatology of snow accumulation. This aligns with the findings of Shulgina et al. (2023), who reported that ARs contribute to 40% of the total seasonal snow in California's snowy mountains, another region with a semi-arid Mediterranean climate. The strong temperature and precipitation changes can result in distinct snowmelt patterns on AR days compared to the climatology (Figs. 5g-h). The accumulation of total snowmelt (ΔSMLT) is about 16 mm in the headwater region on AR days, while it can exceed 40 mm in the lower part of the basin. In contrast, the climatology of total snowmelt exceeds 100 mm in the highland regions in Türkiye and Zagros Mountain ranges, with around 40 mm in the headwater region.

Given that the ET Rivers are crucial water resources supplying multiple transborder countries in the Middle East, understanding hydrometeorological changes in the water tower area during winter is of utmost importance.

**Fig. 5** Intensity of surface air temperature (SAT) changes, accumulation of total precipitation (TP), snow water equivalent SWE, and snowmelt (SMLT) in the winter season for AR days (**a, c, e, g**) and 40-year climatology of these variables (**b, d, f, h**). Accumulation of ΔTP, ΔSWE, ΔT, and ΔSMLT calculated summing values from one day before to one day after an AR event based on daily values and only if Δ (T, TP, SWE, and SMLT) > 0, variables are averaged over the days for each grid
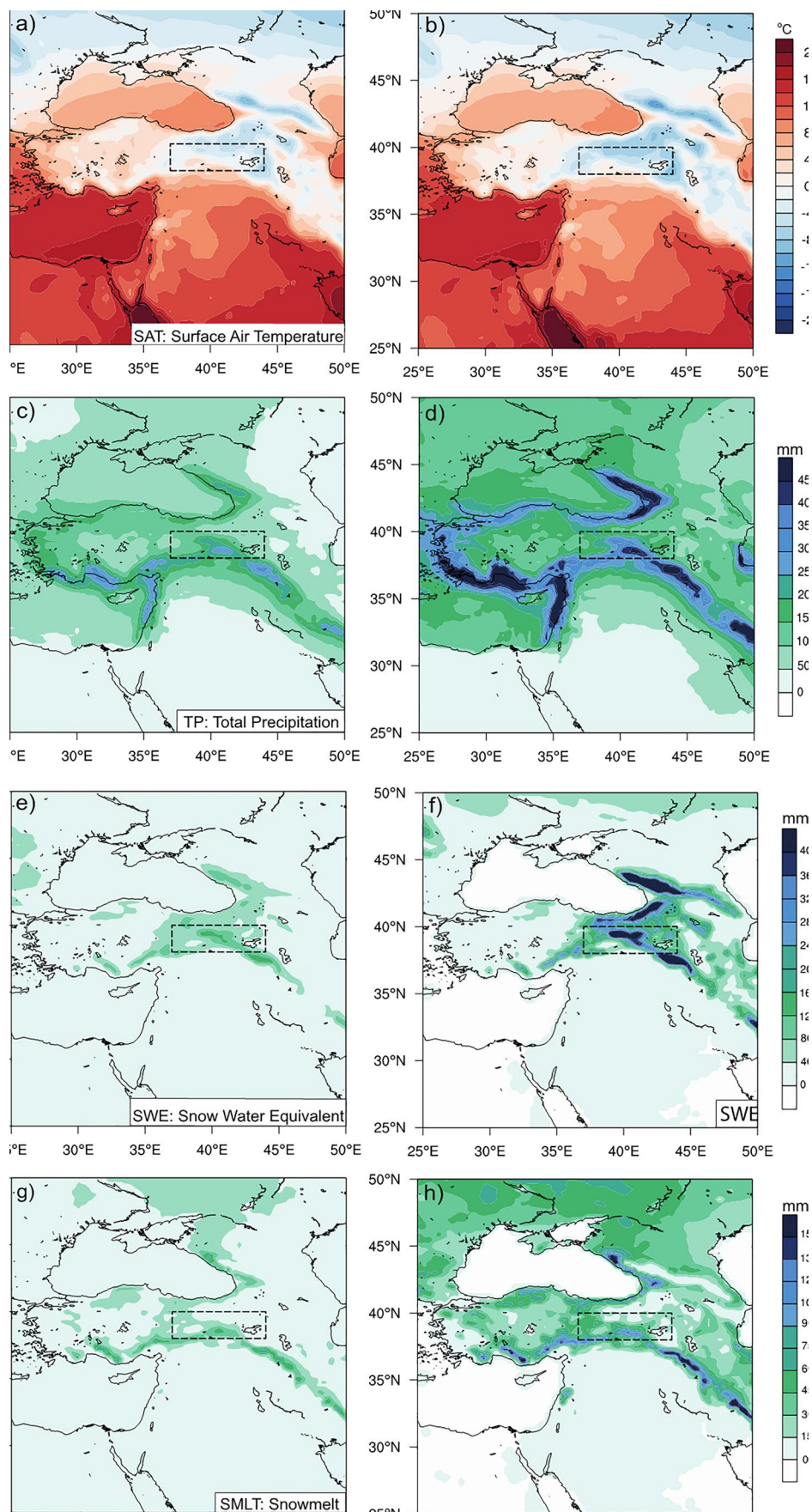
In addition to the aforementioned hydrometeorological changes, surface radiative balance components may also experience alterations during AR events, potentially leading to increased snowpack ablation in snow-dominated regions (Chen et al. 2019; Payne et al. 2020; Zhang et al. 2023). The partition of net shortwave and net longwave radiation under AR and non-AR conditions in the headwater region is presented in Fig. 6a, indicating that mean net shortwave radiation and longwave radiation values are approximately 20 Wm$^{-2}$ higher on non-AR days compared to AR days. Figure 6b indicates that downward shortwave radiation is lower and downward longwave radiation is higher on AR days relative to non-AR days. This suggests that rain-on-snow events, caused by warming or increased downward longwave radiation due to cloudiness, contribute to snowpack ablation. These radiative components indicate that reflected shortwave radiation is high on non-AR days, while upward longwave radiation is high on AR days, supporting snowpack increase on non-AR days and snowmelt increase on AR days. Therefore, the radiative balance components over the headwater region where 51% (~ %93) of the region is above 1700 (1000) meters indicate that the presence of clouds on AR days contributes to snowmelt accumulation due to both radiative and rain-on-snow impacts, in agreement with Figs. 5a, e and g. It is also important to note that SWE loss due to snowmelt could lead to a misinterpretation of the impacts of the rain-on-snow events on the snowpack, as the available energy may not be adequate for such SWE loss. To fully understand the impacts of rainfall on snow, additional factors such as soil moisture, streamflow, snow cover structure,

and precipitation phase must be considered alongside the energy balance (Haleakala et al. 2022).

The relationship between total precipitation and altitude on AR days is plotted using the 2 °C temperature threshold as the transition temperature between rain and snow in Fig. 6c (Bonan 1996; Dingman 2002). Specifically, if the temperature falls below the 2 °C threshold value, the total precipitation is classified as snow. If the temperature is above 2 °C, the total precipitation is categorized as rainfall. The clustering of total precipitation based on altitude in the headwater area shows that precipitation is in the form of rain below approximately 1200 m and snow above 1200 m, according to the threshold value.

### 3.3.1 AR-related interannual changes in hydrometeorology of the headwater region

In the previous sections, we have presented the hydrometeorological impacts of winter AR conditions in the eastern Mediterranean region, specifically focusing on the headwater region of the ET Basin, from a climatological perspective. In this subsection, our objective is to examine how surface winter hydrometeorological variables vary from year to year under AR conditions in the headwater region.

Temperatures generally remain below 0 °C on AR days in winter (Fig. 7a). Nonetheless, they rise above 0 °C in certain years (i.e., 1982, 1984, 1989, 1991,1997, 1999, 2010, 2015, and 2018). On non-AR days, temperatures never exceed 0 °C (Fig. 7b).

Under non-AR conditions, total precipitation generally ranges from 40 to 100 mm, whereas under AR conditions,
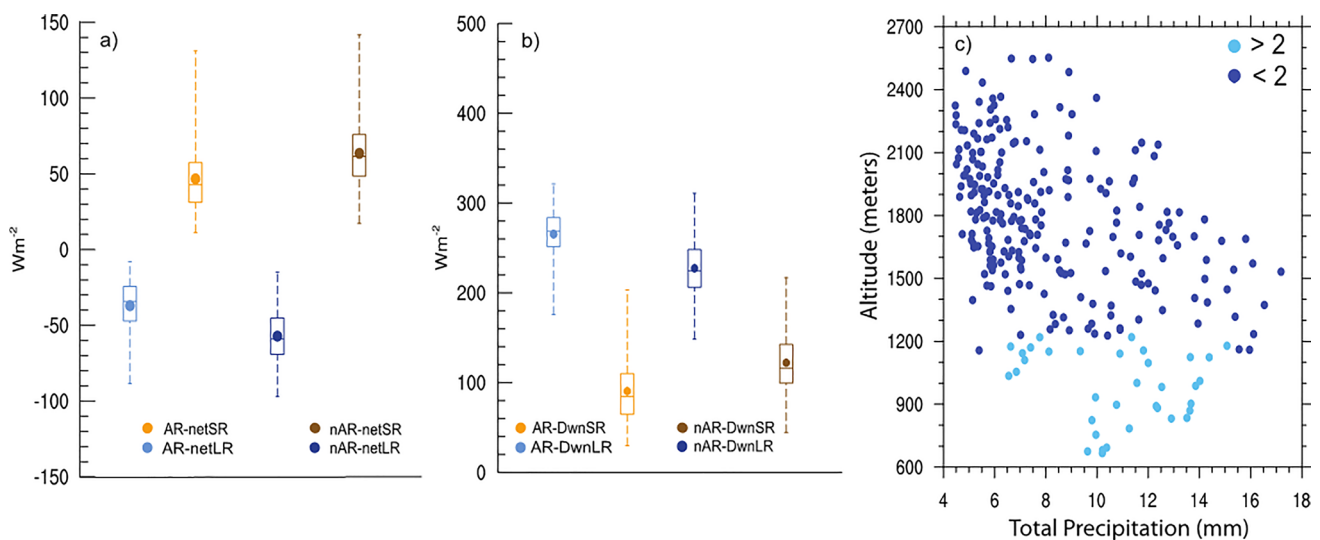


**Fig. 6** Net shortwave and longwave radiation for AR (AR-netSR and AR-netLR) and non-AR (nAR-netSR and nAR-netLR) days (**a**), downward short and longwave radiation (**b**) for AR (AR-DwnSR and AR-DwnLR) and non-AR (nAR-DwnSR and nAR-DwnLR) days, and scatter plot of total precipitation associated with altitude above and below 2 °C temperature over the headwater region on AR days for DJF (**c**)

upper range of precipitation approximately doubles, reaching around 200 mm (e.g., in years 1987, 1988, 2004, 2010, 2013, and 2019) (Figs. 7c and d). The average winter SWE amount on AR days (~ 58 mm) during the period of 1979–2019 is slightly lower than on non-AR days (average of ~ 62 mm) (Figs. 7e and f). There is no specific year-to-year pattern regarding SWE for either condition. However, the overall snow amount in the region has decreased over time. Shulgina et al. (2023) noted that snow accumulation in California's snowy mountains may decline to less than half of its historical value by the late twenty-first century, with the greatest losses occurring at mid-altitudes. Thus, this characteristic may become even more important in the future due to unabated warming. Snowmelt is a bit more pronounced under AR conditions compared to non-AR conditions (Figs. 7g and h). During the 1979–2019 winters, the average snowmelt is approximately 23 mm (18 mm) under AR (non-AR) conditions. Notably, a significant amount of snowmelt (~ 80 mm) occurred in 2010, a year with high precipitation (reaching around 250 mm) and an average temperature exceeding 1.5 °C. In the following subsection, we present more details about the hydrometeorological conditions in 2010 winter.

### 3.3.2 Influential AR days over the region in the winter of 2010

Here, we focus specifically on the winter of 2010 due to the remarkable relationship between precipitation, temperature, and snowmelt in the headwater region. Figure 8a provides an overview of the 40-year winter climatology of the shortwave and longwave radiation components compared to those in the year 2010. In 2010, the region received higher average solar radiation (~ 80 Wm$^{-2}$) compared to the climatology, while the emitted longwave radiation remains almost the same (~ -40 Wm$^{-2}$). Furthermore, the high downward shortwave and longwave radiation in 2010 compared to the 40-year climatology, respectively indicated a warmer and cloudier lower atmosphere in the headwater region (Fig. 8b). This is consistent with the high precipitation (~ 260 mm season$^{-1}$) and snowmelt (~ 80 mm season$^{-1}$) as well as the high temperature (+ 1.5 °C/season) and low SWE on AR days in Fig. 7. The average temperature of the headwater region shown by the dashed box in Fig. 5 is lower than the threshold value (2 °C), however, it might rise over 2 °C depending on the altitude, which triggers snowmelt in different parts of the headwater region. Consequently, the snow cover decreased due to relatively high temperatures and rain-on-snow effect in 2010.

We conducted a transect analysis to look into the temperature and humidity fields along a line crossing eastern Anatolia in the meridional direction, which reveals that the winter of 2010 is about 2 °C warmer than the climatology in the southern plains over Mesopotamia and the Black

Sea side of the Anatolian Peninsula (point B). The warm air advection in the lower atmosphere extends to the upper layers during the year 2010 (Fig. 8d). The warming effect is evident up to 700 hPa (Figs. 8c and d). In addition, the year 2010 winter exhibits higher humidity in the air compared to the climatology, and the higher positive vertical velocity (upward motion is associated with negative velocity values in ERA5) indicates increased subsidence, which explains the temperature rise in 2010.

February 2010 was a month characterized by prolonged AR events. We focus on the day 21 February 2010, when the IVT reached a pretty high value (260 kg m$^{-1}$ s$^{-1}$ > 99%) compared to the monthly IVT values for the 40-yr period. Figure 9a illustrates the 6-hourly AR axes obtained from the AR catalog on 21 February 2010, traversing northern Africa and bringing relatively warm air masses to the Anatolian Peninsula. A deep upper-level trough over the Atlantic Ocean and a strong ridge in northeastern Africa and the Arabian Peninsula on 21 February create favorable conditions for a relatively strong transport of dry-warm African air to the Euro-Mediterranean region (Fig. 9b). The temperature anomaly of the day (Fig. 9c) supports the intrusion of warm air into the Euro-Mediterranean, reaching up to + 8–9 °C depending on the area. In contrast to the eastern Mediterranean, cold temperature anomalies (~ -4 °C) in western Europe indicate a dipole pattern, similar to the findings of Bozkurt et al. (2021) over a similar domain.

A southwest-northeast-oriented AR brings wetter conditions (ranging from + 2 mm day$^{-1}$ to + 10 mm day$^{-1}$) to the western and central parts of Türkiye (Fig. 9d). However, the decrease in SWE over these regions reveals that the increase in precipitation mostly occurs in the form of rain. Therefore, the rain-on-snow effect appears to be dominant in these regions (Fig. 9e). On the contrary, precipitation in the form of snow over some highland regions of the eastern Black Sea Mountains, Zagros Mountains, and headwater region helps to increase snow accumulation (SWE ~ 2–4 cm day$^{-1}$) since the temperatures at those high altitudes are low enough to produce snowfall. Furthermore, snow depletion and drier conditions on AR days over the immediate highlands encircling the Fertile Crescent, an important agricultural region for the Middle East, are notable.

## 4 Discussion and conclusions

In this study, we examined the characterization of wintertime ARs and their impacts on the snowpack in eastern Anatolia, where the headwaters of the ET Basin are located, using a state-of-the-art AR catalog (Guan and Waliser 2019) and ERA5 reanalysis dataset for the period 1979–2019. Our
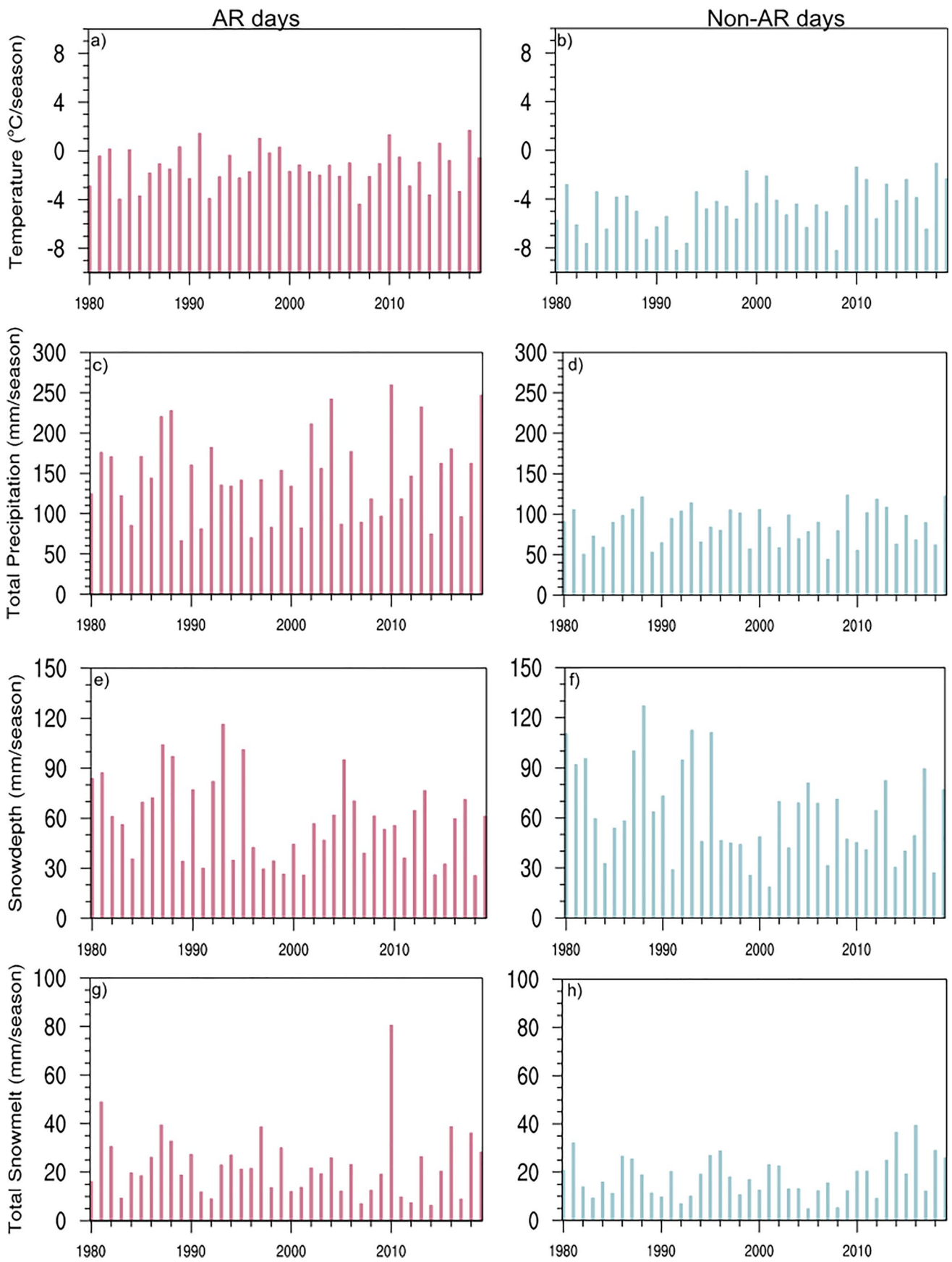
◄**Fig. 7** Interannual changes of temperature, total precipitation, snow water equivalent, and snowmelt over the headwater region in the winter season for AR-days (**a**, **c**, **e** and **g**) and non-AR days (**b**, **d**, **f** and **h**)

analysis reveals several important findings regarding the wintertime AR characteristics and impacts in the region.

We found that the frequency of the ARs during the winter season in eastern Anatolia is 2–4 days, with higher frequency detected during the transition seasons. However, the ARs in the headwater regions are relatively weak. Synoptic weather patterns associated with winter ARs are generally similar to those depicted in the melting season (Bozkurt et al. 2021), with a stronger Mediterranean trough and an anticyclone over the Caspian Sea. In addition, the location of the African subtropical jet shifts from the west (during the snowmelt season) to the east of Africa on winter AR days.

Temperature and precipitation anomalies indicate that AR days in the headwater region can be warmer by up to 3 °C and wetter by over 5 mm day$^{-1}$ compared to climatology. The contribution of ARs to the seasonal total precipitation varies from year to year, with the maximum contribution (over 80%) in 2010 and the minimum contribution (around 40%) in 2009. On average, ARs account for around 60% of the seasonal total precipitation in the basin, with an average total precipitation accumulation of around 8 mm day$^{-1}$ on AR days. Snow contributions on AR days exhibit spatial variability, with an increase in SWE up to 3 mm day$^{-1}$ in the upper headwater region and a decrease in the remaining parts of the basin. The average snow accumulation on AR days is approximately 4 mm day$^{-1}$ over the headwater basin, and ARs contribute to 27% of the seasonal average snow accumulation. The contribution of ARs to the snowpack ranges from 12% in 1989 to 57% in 2010 for the region. It has been shown that AR events play an important role in snow accumulation and contribute to between 43 and 51% of total snow accumulation in the extratropical Andes of South America (Saavedra et al. 2020; Viale et al. 2018). In addition, Huning et al. (2017, 2019) estimated 52–62% and Guan et al. (2010, 2013) found a 30–40% AR contribution to snow in the Sierra Nevada of California, USA. Shulgina et al. (2023) concluded that due to their warmth characteristics, AR storms produce higher snowlines, contributing 40% of total seasonal snow than non-AR storms in California's snowy mountains. Comparing our results to previous studies, the snow contribution from ARs in the Anatolian highlands (27%) is reasonable, considering that the region's elevation is not as high as the Andes or the Sierra Nevada, and the intensity of IVT carried by ARs this far inland is not as strong as that associated with those originating from the Pacific Ocean. Although ARs are not effective for snow accumulation in the Anatolian plateau, rain-on-snow events have more potential to occur, which can increase the risk of flooding, due to the contribution of over 60% of the total precipitation in the region.

The discrepancy (high total precipitation contribution and low snowpack contribution) suggests that ARs play a crucial role in enhancing overall precipitation in the region. The high total precipitation contribution can be attributed to the semi-arid characteristics of the study area. Eastern Anatolia is known for its arid to semi-arid climate (Turkes 1998, 2003), characterized by limited rainfall and moisture availability. However, when winter ARs interact with the region, they bring a significant amount of moisture and trigger precipitation enhancement. Additionally, the complex terrain of the region, including the presence of mountains, plays a role in triggering orographic lifting (Turkes et al. 2009; Onol and Unal 2012). As the moisture-laden air encounters the mountain ranges, it is forced to rise, leading to orographic precipitation. This process further enhances the total precipitation during AR events. The combination of the semi-arid climate, the presence of a low-level jet, and orographic lifting provide favorable conditions for precipitation enhancement during AR events in eastern Anatolia. While the snow contribution may be relatively low, the overall total precipitation contribution from ARs highlights their importance in replenishing water resources. The high precipitation and low snowpack contribution during AR events in the region can be attributed to rain-on-snow events, where rain falling on existing snow rapidly melts the snowpack and contributes to increased runoff (Bozkurt et al. 2021).

Notably, the south-facing parts of the mountain range experience significant snowmelt, with the minimum and maximum snowmelt contributions occurring in 2014 (15%) and 2010 (80%), respectively. Approximately 30 Wm$^{-2}$ less downward shortwave radiation and 40 Wm$^{-2}$ greater downward longwave radiation on AR days compared to non-AR days point to the presence of cloudy skies on AR days and snow on non-AR days in the region. We highlight that rain on AR days generally tends to form over the regions where the altitude is below 1200 m for the headwater region.

The interannual variability of hydrometeorological variables highlighted the exceptional nature of the year 2010. Despite only + 1.5 °C temperature deviation from the seasonal average, total precipitation in 2010 accounted for 57% of the seasonal total and 80% of the snowmelt. These changes underscore the significant impact of the rain-on-snow process associated with ARs in shaping the climate conditions of that year. A particularly extreme AR event observed in February further highlighted the rain-on-snow effect, leading to snow depletion, although the snow contribution remained influential in a small area within the upper part of the headwater region of the ET Basin.

In light of our findings, several recommendations can be made. Firstly, continued monitoring and research on ARs in the region are necessary to better understand their
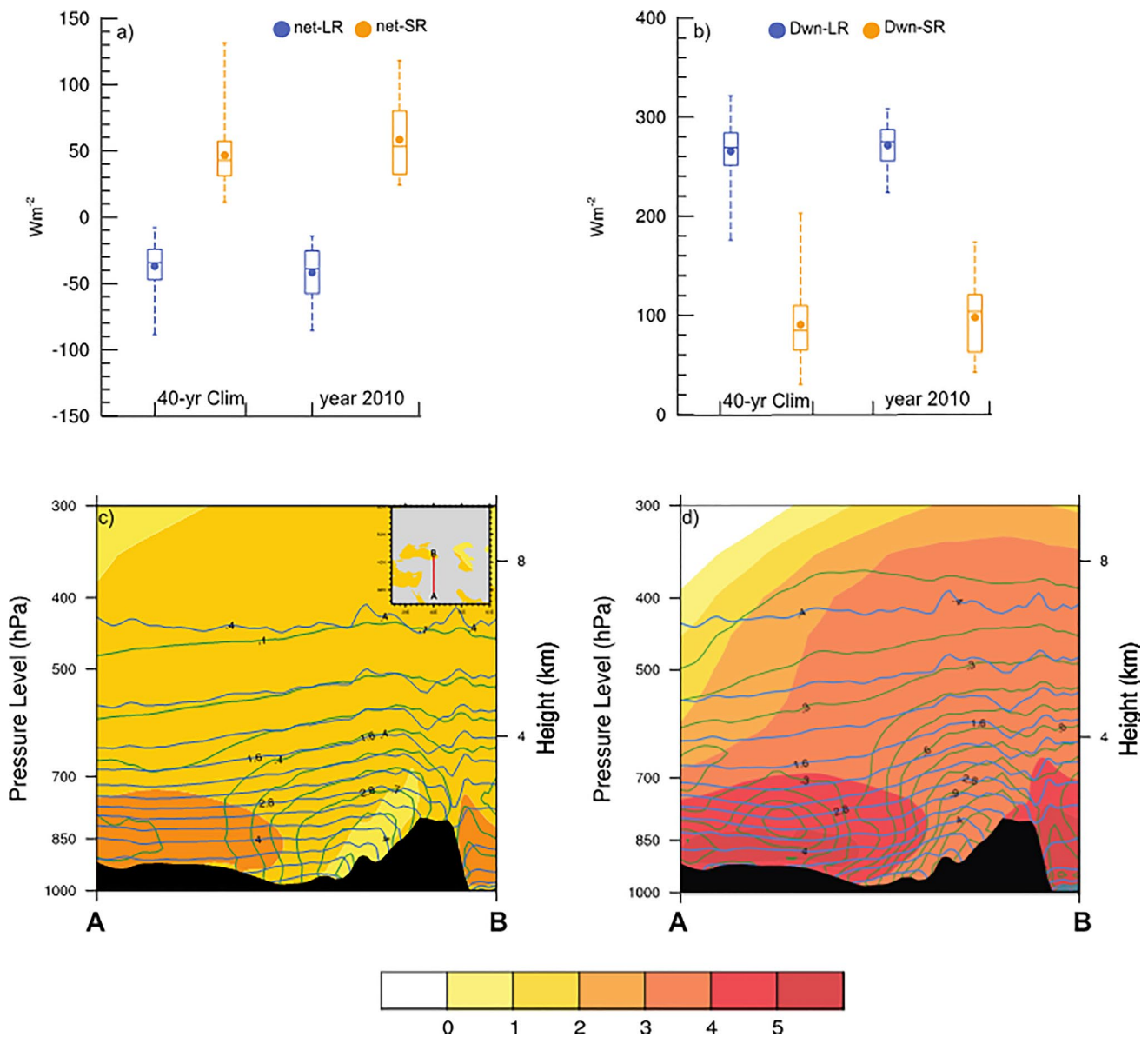
**Fig. 8** Net shortwave and longwave radiations (**a**) and downward shortwave and long wave radiation (**b**) on winter AR days for 40-year climatology and the year 2010. Vertical profile of potential tempera-ture (shaded), vertical velocity (blue contours), and specific humidity (green contours) anomalies along a north–south transect for (**c**) 40-year (1979–2019) climatology, and (**d**) the year 2010

spatiotemporal characteristics and their impact on snow-pack dynamics. This would involve further analysis of AR intensity, duration, and moisture transport patterns, as well as their interactions with local topography, includ-ing numerical modeling efforts. Secondly, considering the potential implications of AR-induced snowmelt, it is cru-cial to assess the water resource management strategies in the ET Basin. The findings of this study highlight the importance of accounting for the contribution of ARs to the overall water availability and planning for potential changes in snowpack dynamics. Further research is also warranted to improve our understanding of the projected

hydroclimate changes in Mediterranean climate regions (e.g., Polade et al. 2017; Bozkurt and Sen 2013) and the role of ARs in the changing hydroclimate (e.g., Gershunov et al. 2019) as well as on projected snowline and snow accumulation (e.g., Shulgina et al. 2023). In this context, it is also important to improve the representation of ARs and their associated rain-on-snow effect in climate models. This will enable more accurate predictions of snow accu-mulation, snowmelt, and water availability in the region, especially considering the potential implications for agri-culture, hydroelectric power generation, and overall water resource management.
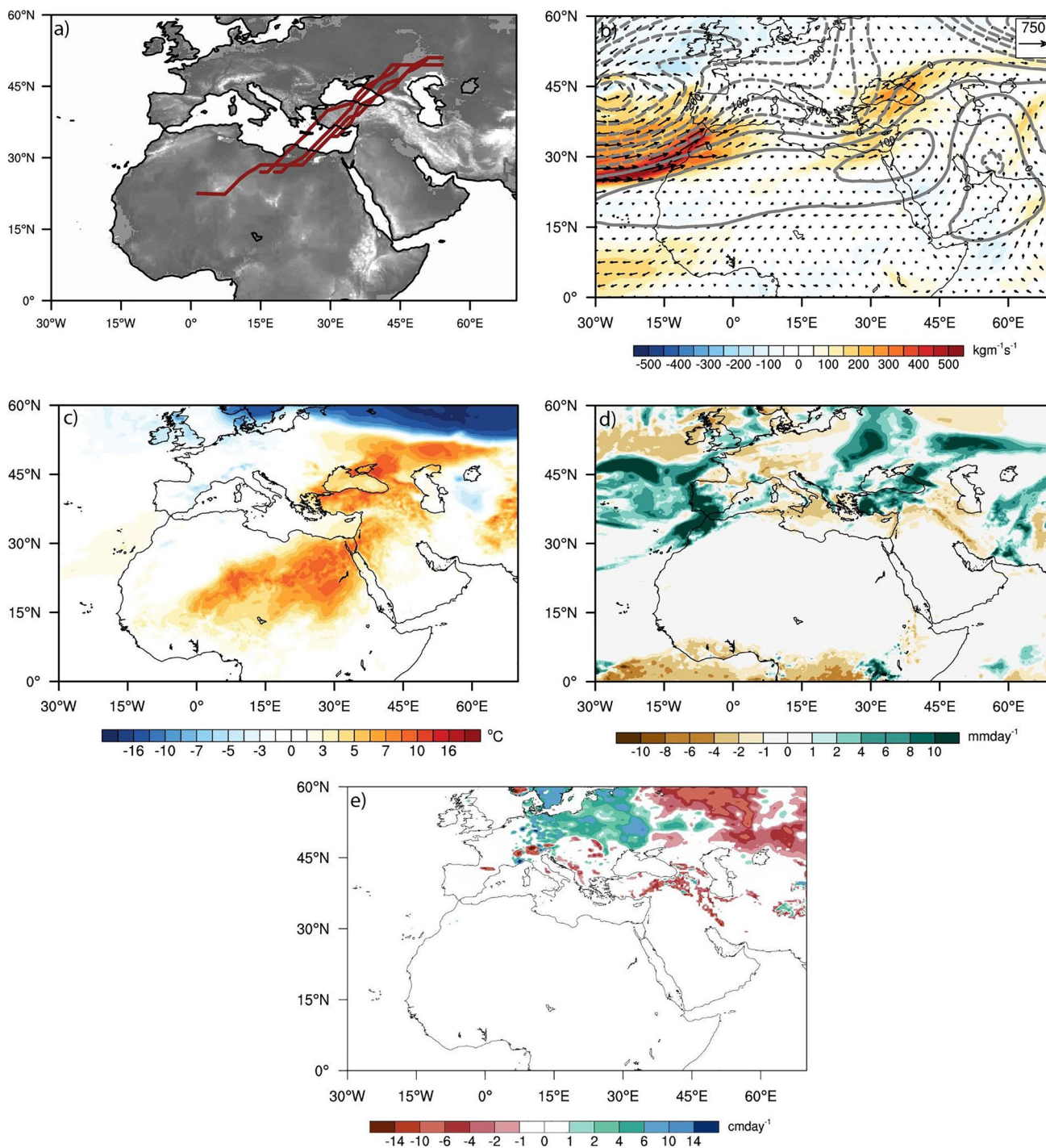
**Fig. 9** **a** AR axes for every 6 h, and anomalies of **b**) IVT (shaded) and 500 hPa (contours), **c** 2-m temperature, **d** precipitation, and **e**) SWE on February 21 2010

Despite the insights provided by this study, there are some caveats to consider. The region of interest includes important limitations associated with the coverage of observed data (e.g., limited spatial density of stations, short record lengths, lack of observations at higher elevations, etc.), which are subject to inherent uncertainties.

Another limitation pertains to the reliability of the reanalysis data. The AR catalog has not been updated for the new high-resolution reanalysis dataset (ERA5). Additionally, the precipitation and snow information obtained from ERA5 lacks sufficient resolution to adequately assess the rugged topographic barrier regions. Future research could

benefit from incorporating more high-resolution numerical models, local observations, and field campaigns to improve the accuracy of the results.

In conclusion, this study enhances our understanding of the contribution of winter ARs to the snowpack in eastern Anatolia. It highlights the spatial and temporal changes in AR activity, their impact on temperature, precipitation, and snow accumulation, and remarks the potential role of the rain-on-snow effect in shaping the regional climate. The findings have implications for water resource management and call for continued research to improve our knowledge of ARs and their interactions with the complex terrain of the ET Basin.

## Declarations

## References

Akbary M, Salimi S, Hosseini SA, Hosseini M (2019) Spatio-temporal changes of atmospheric rivers in the Middle East and North Africa region. Int J Climatol 39(10):3976–3986. https://doi.org/10.1002/joc.6052

American Meteorological Society (2024) Atmospheric river. Glossary of Meteorology. https://glossary.ametsoc.org/wiki/Atmospheric_river. Accessed 5 Aug 2023

Batibeniz F, Ashfaq M, Önol B et al (2020) Identification of major moisture sources across the Mediterranean Basin. Clim Dyn 54:4109–4127. https://doi.org/10.1007/s00382-020-05224-3

Bonan GB (1996) A Land Surface Model (LSM version 1.0) for ecological, hydrological, and atmospheric studies: Technical description and user's guide, NCAR Technical. Note NCAR/TN-417+STR. National Center for Atmospheric Research, Boulder, CO, p 91

Bozkurt D, Sen OL (2011) Precipitation in the Anatolian Peninsula: sensitivity to increased SSTs in the surrounding seas. Clim Dyn 36(3–4):711–726. https://doi.org/10.1007/s00382-009-0651-3

Bozkurt D, Sen OL (2013) Climate change impacts in the Euphrates-Tigris Basin based on different model and scenario simulations. J Hydrol 480:149–161. https://doi.org/10.1007/s00382-009-0651-3

Bozkurt D, Ezber Y, Sen OL (2019) Role of the East Asian Trough on the Eastern Mediterranean temperature variability in early spring and the extreme case of 2004 warm spell. Clim Dynamics 53(3):2309–2326. https://doi.org/10.1007/s00382-019-04847-5

Bozkurt D, Sen OL, Ezber Y, Guan B, Viale M, Caglar F (2021) Influence of African atmospheric rivers on precipitation and snowmelt in the Near East's highlands. J Geophys Res: Atmos 126:e2020JD033646. https://doi.org/10.1029/2020JD033646

Chen X, Leung LR, Wigmosta M, Richmond M (2019) Impact of atmospheric rivers on surface hydrological processes in western U.S. watersheds. J Geophys Res: Atmos 124:8896–8916. https://doi.org/10.1029/2019JD030468

Cordeira JM, Stock J, Dettinger MD, Young AM, Kalansky JF, Ralph FM (2019) 142-Year Climatology of Northern California Landslides and Atmospheric Rivers. Bull Am Meteorol Soc 100(8):1499–1510

Corringham TW, Ralph FM, Gershunov A, Cayan DR, Talbot CA (2019) Atmospheric rivers drive flood damages in the western United States. Sci Adv 5(12):eaax4631. https://doi.org/10.1126/sciadv.aax4631

De Luca P, Hillier JK, Wilby RL, Quinn NW, Harrigan S (2017) Extreme multi-basin flooding linked with extra-tropical cyclones. Environ Res Lett 12(11):114009

de Vries AJ, Ouwersloot HG, Feldstein SB, Riemer M, El Kenawy AM, McCabe MF, Lelieveld J (2018) Identification of tropical-extratropical interactions and extreme precipitation events in the Middle East based on potential vorticity and moisture transport. J Geophys Res: Atmos 123:861–881. https://doi.org/10.1002/2017JD027587

Dettinger MD, Ralph FM, Das T, Neiman PJ, Cayan DR (2011) Atmospheric rivers, floods and the water resources of California. Water 3:445–478. https://doi.org/10.3390/w3020445

Dezfuli A (2020) Rare atmospheric river caused record floods across the Middle East. Bull Am Meteor Soc 101(4):E394–E400. https://doi.org/10.1175/BAMS-D-19-0247.1

Dingman SL (2002) Physical Hydrology, 2nd edn. Prentice-Hall, Upper Saddle River, p 108

Esfandiari N, Lashkari H (2021) The effect of atmospheric rivers on cold-season heavy precipitation events in Iran. J Water Clim Chang 12(2):596–611. https://doi.org/10.2166/wcc.2020.259

Francis D, Fonseca R, Nelli N, Bozkurt D, Cuesta J, Bosc E (2022) On the Middle East's severe dust storms in spring 2022: Triggers and impacts. Atmos Environ 296:119539. https://doi.org/10.1016/j.atmosenv.2022.119539

Gershunov A, Shulgina TM, Clemesha RES, Guirguis K, Pierce DW, Dettinger MD, Lavers DA, Cayan DR, Polade SD, Kalansky J, Ralph FM (2019) Precipitation regime change in Western North America: The role of Atmospheric Rivers. Nat Sci Rep 9:9944. https://doi.org/10.1038/s41598-019-46169-whttps://rdcu.be/bJPK0

Guan B, Waliser DE (2015) Detection of atmospheric rivers: Evaluation and application of an algorithm for global studies. J Geophys Res Atmos 120(24):12514–12535. https://doi.org/10.1002/2015JD024257

Guan B, Waliser DE (2019) Tracking atmospheric rivers globally: Spatial distributions and temporal evolution of life cycle characteristics. J Geophys Res Atmos 124(23):12523–12552. https://doi.org/10.1029/2019JD031205

Guan B, Molotch NP, Waliser DE, Fetzer EJ, Neiman PJ (2010) Extreme snowfall events linked to atmospheric rivers and surface air temperature via satellite measurements. Geophys Res Lett 37:2–7. https://doi.org/10.1029/2010GL044696

Guan B, Molotch NP, Waliser DE, Fetzer EJ, Neiman PJ (2013) The 2010/2011 snow season in California's Sierra Nevada: role of atmospheric rivers and modes of large-scale variability. Water Resour Res 49:6731–6743. https://doi.org/10.1002/wrcr.20537

Guan B, Waliser DE, Ralph FM, Fetzer EJ, Neiman PJ (2016) Hydrometeorological characteristics of rain-on-snow events associated with atmospheric rivers. Geophys Res Lett 43(6):2964–2973. https://doi.org/10.1002/2016GL067978

Guan B, Waliser DE, Ralph FM (2018) An intercomparison between reanalysis and dropsonde observations of the total water vapor transport in individual atmospheric rivers. J Hydrometeorol 19:321–337. https://doi.org/10.1175/JHM-D-17-0114

Hecht CW, Cordeira JM (2017) Characterizing the influence of atmospheric river orientation and intensity on precipitation distributions over North Coastal California. Geophys Res Lett 44:9048–9058. https://doi.org/10.1002/2017GL074179

Hersbach H, Bell B, Berrisford P, Biavati G, Horányi A, Muñoz Sabater J, Nicolas J, Peubey C, Radu R, Rozum I, Schepers D, Simmons A, Soci C, Dee D, Thépaut J-N (2023) ERA5 hourly data on pressure levels from 1940 to present. Copernicus Climate Change Service (C3S) Climate Data Store (CDS). https://doi.org/10.24381/cds.bd0915c6

Huning LS, Margulis SA, Guan B, Waliser DE, Neiman PJ (2017) Implications of detection methods on characterizing atmospheric river contribution to seasonal snowfall across Sierra Nevada, USA. Geophys Res Lett 44(20):10445–10453. https://doi.org/10.1002/2017GL075201

Huning LS, Guan B, Waliser DE, Lettenmaier DP (2019) Sensitivity of seasonal snowfall attribution to atmospheric rivers and their reanalysis-based detection. Geophys Res Lett 46:794–803. https://doi.org/10.1029/2018GL080783

Junker NW, Grumm RH, Hart R, Bosart LF, Bell KM, Pereira FJ (2008) Use of normalized anomaly fields to anticipate extreme rainfall in the mountains of northern California. Weather Forecast 23(3):336–356. https://doi.org/10.1175/2007WAF2007013.1

Kim J, Waliser DE, Neiman PJ, Guan B, Ryoo J-M, Wick GA (2013) Effects of atmospheric river landfalls on the cold season. Clim Dyn 40:465–474. https://doi.org/10.1007/s00382-012-1322-3

Lavers DA, Villarini G (2015) The contribution of atmospheric rivers to precipitation in Europe and the United States. J Hydrol 522:382–390. https://doi.org/10.1016/j.jhydrol.2014.12.010

Lavers DA, Allan RP, Wood EF, Villarini G, Brayshaw DJ, Wade AJ (2011) Winter floods in Britain are connected to atmospheric rivers. Geophys Res Lett 38:1–8. https://doi.org/10.1029/2011GL049783

Lavers DA, Villarini G, Allan RP, Wood EF, Wade AJ (2012) The detection of atmospheric rivers in atmospheric reanalyses and their links to British winter floods and the large-scale climatic circulation. J Geophys Res Atmos 117:1–13. https://doi.org/10.1029/2012JD018027

Leung LR, Qian Y (2009) Atmospheric rivers induced heavy precipitation and flooding in the western U.S. simulated by the WRF regional climate model. Geophys Res Lett 36:L03820. https://doi.org/10.1029/2008GL036445

Lolis CJ, Türkeş M (2016) Atmospheric circulation characteristics favouring extreme precipitation in Turkey. Clim Res 71(2):139–153. https://doi.org/10.3354/cr01433

Lorente-Plazas R, Montavez JP, Ramos AM, Jerez S, Trigo RM, Jimenez-Guerrero P (2020) Unusual atmospheric-river-like structures coming from Africa induce extreme precipitation over the western Mediterranean Sea. J Geophys Res Atmos 125(2):e2019JD031280. https://doi.org/10.1029/2019JD031280

Nayak MA, Villarini G (2017) A long-term perspective of the hydroclimatological impacts of atmospheric rivers over the central United States. Water Resour Res 53:1144–1166. https://doi.org/10.1002/2016WR019033

Neiman PJ, Ralph FM, White AB, Kingsmill DE, Persson POG (2002) The statistical relationship between upslope flow and rainfall in California's coastal mountains: Observations during CALJET. Mon Weather Rev 130:1468–1492

Neiman PJ, Ralph FM, Wick GA, Lundquist JD, Dettinger MD (2008) Meteorological characteristics and overland precipitation impacts of atmospheric rivers affecting the West Coast of North America based on eight years of SSM/I satellite observations. J Hydrometeor 9:22–47. https://doi.org/10.1175/2007JHM855.1

Neiman PJ, Schick LJ, Ralph FM, Hughes M, Wick GA (2011) Flooding in Western Washington: the connection to atmospheric rivers. J Hydrometeorol 12:1337–1358. https://doi.org/10.1175/2011JHM1358.1

Oakley NS, Liu T, McGuire LA, Simpson M, Hatchett BJ, Tardy A, Kean JW, Castellano C, Laber JL, Steinhoff D (2023) Toward probabilistic post-fire debris-flow hazard decision support. Bull Am Meteorol Soc 104(9):E1587–E1605. https://doi.org/10.1175/BAMS-D-22-0188.1

Onol B, Unal YS (2012) Assessment of climate change simulations over climate zones of Turkey. Reg Environ Change 14:1921–1935. https://doi.org/10.1007/s10113-012-0335-0

Payne AE, Demory M, Leung LR, Ramos AM, Shields CA, Rutz JJ, Ralph FM (2020) Responses and impacts of atmospheric rivers to climate change. Nat Rev Earth Environ 1(3):143–157. https://doi.org/10.1038/s43017-020-0030-5

Polade SD, Gershunov A, Cayan DR, Dettinger MD, Pierce DW (2017) Precipitation in a warming world: Assessing projected hydro-climate of California and other Mediterranean climate regions. Nat Sci Rep 7:10783. https://doi.org/10.1038/s41598-017-11285-y

Ralph FM, Neiman PJ, Wick GA (2004) Satellite and CALJET aircraft observations of atmospheric rivers over the eastern North Pacific Ocean during the winter of 1997/98. Mon Wea Rev 132:1721–1745. https://doi.org/10.1175/1520-0493(2004)132,1721:SACAOO.2.0.CO;2

Ralph FM, Neiman PJ, Rotunno R (2005) Dropsonde Observations in Low-Level Jets over the Northeastern Pacific Ocean from CALJET-1998 and PACJET-2001: Mean Vertical-Profile and Atmospheric-River Characteristics. Mon Wea Rev 133:889–909

Ralph FM, Neiman PJ, Wick GA, Gutman SI, Dettinger MD, Cayan DR et al (2006) Flooding on California's Russian River: Role of atmospheric rivers. Geophys Res Lett 33:L13801. https://doi.org/10.1029/2006GL026689

Ralph FM, Rutz JJ, Cordeira JM, Dettinger M, Anderson M, Reynolds D, Schick LJ, Smallcomb C (2019) A scale to characterize the strength and impacts of atmospheric rivers. Bull Am Meteorol Soc 100(2):269–289. https://doi.org/10.1175/BAMS-D-18-0023.1

Ramos AM, Trigo RM, Tomé R, Liberato MLR (2018) Impacts of atmospheric rivers in extreme precipitation on the European Macaronesian Islands. Atmosphere 9(8):325. https://doi.org/10.3390/atmos9080325

Ridder N, de Vries H, Drijfhout S (2018) The role of atmospheric rivers in compound events consisting of heavy precipitation and high storm surges along the Dutch coast. Nat Hazards Earth Syst Sci 18:3311–3326. https://doi.org/10.5194/nhess-18-3311-2018

Rössler O, Froidevaux P, Börst U, Rickli R, Martius O, Weingartner R (2014) Retrospective analysis of a nonforecasted rain-on-snow flood in the Alps—A matter of model limitations or unpredictable nature? Hydrol Earth Syst Sci 18:2265–2285. https://doi.org/10.5194/hess-18-2265-2014

Rutz J, Steenburgh WJ (2012) Quantifying the role of atmospheric rivers in the interior western United States. Atmos Sci Let 13:257–261. https://doi.org/10.1002/asl.392

Rutz JJ, Steenburgh WJ, Ralph FM (2014) Climatological characteristics of atmospheric rivers and their inland penetration over the Western United States. Mon Weather Rev 142(2):905–921. https://doi.org/10.1175/MWR-D-13-00168.1

Saavedra F, Cortés G, Viale M, Margulis S, McPhee J (2020) Atmospheric Rivers Contribution to the Snow Accumulation Over the Southern Andes (265° S–375° S). Front Earth Sci 8:261. https://doi.org/10.3389/feart.2020.00261

Sadeghi M et al. (2021) Application of remote sensing precipitation data and the CONNECT algorithm to investigate spatiotemporal variations of heavy precipitation: case study of major floods across Iran (Spring 2019), J. Hydrol., 600, https://www.sciencedirect.com/science/article/pii/S0022169421006168

Sen OL, Ezber Y, Bozkurt D (2019) Euro-Mediterranean climate variability in boreal winter: A potential role of the East Asian Trough. Clim Dyn 52(10):7071–7084. https://doi.org/10.1007/s00382-018-4573-9

Shulgina T, Gershunov A, Hatchett B, Guirguis K, Subramanian AC, Margulis SA, Fang Y, Cayan DR, Pierce DW, Dettinger M, Anderson ML, Ralph FM (2023) Observed and projected changes in snow accumulation and snowline in California's snowy mountains. Clim Dyn 61:4809–4824. https://doi.org/10.1007/s00382-023-06776-w

Turkes M (1998) Influence of geopotential heights, cyclone frequency and Southern Oscillation on rainfall variations in Turkey. Int J Climatol 18:649–680

Turkes M, Koc T, Sarış F (2009) Spatiotemporal variability of precipitation total series over Turkey. Int J Climatol 29:1056–1074. https://doi.org/10.1002/joc.1768

Turkes M (2003) Spatial and temporal variations in precipitation and aridity index series of Turkey. In: Bolle HJ (ed) Mediterranean climate. Regional Climate Studies. Springer, Heidelberg. https://doi.org/10.1007/978-3-642-55657-9_11

Viale M, Valenzuela R, Garreaud RD, Ralph FM (2018) Impacts of atmospheric rivers on precipitation in southern South America. J Hydrometeorol 19:1671–1687. https://doi.org/10.1175/JHM-D-18-0006.1

Waliser D, Guan B (2017) Extreme winds and precipitation during landfall of atmospheric rivers. Nat. Geosci. 10:179–183. https://doi.org/10.1038/ngeo2894

Warner MD, Mass CF, Salathé EP Jr (2012) Wintertime extreme precipitation events along the Pacific Northwest coast: Climatology and synoptic evolution. Mon Wea Rev 140:2021–2043. https://doi.org/10.1175/MWR-D-11-00197.1

Xiong Y, Chen Q, Ren X (2019) Influence of boreal winter intraseasonal variation of Aleutian low on water vapor transport and atmospheric rivers. Atmosphere (basel) 10:1–13. https://doi.org/10.3390/atmos10020049

Yang Y, Zhao T, Ni G, Sun T (2018) Atmospheric rivers over the Bay of Bengal lead to northern Indian extreme rainfall. Int J Climatol 38(2):1010–1021

Yilmaz YA, Aalstad K, Sen OL (2019) Multiple remotely sensed lines of evidence for a depleting seasonal snowpack in the Near East. Remote Sensing 11(5):483. https://doi.org/10.3390/rs11050483

Zhang Z, Ralph FM, Zheng M (2019) The relationship between extratropical cyclone strength and atmospheric river intensity and position. Geophys Res Lett 46:1814–1823. https://doi.org/10.1029/2018GL079071

Zhang P, Chen G, Ting M et al (2023) More frequent atmospheric rivers slow the seasonal recovery of Arctic Sea ice. Nat Clim Chang 13:266–273

Zhu Y, Newell RE (1998) A proposed algorithm for moisture fluxes from atmospheric rivers. Mon Wea Rev 126:725–735

**Publisher's Note** Springer Nature remains neutral with regard to jurisdictional claims in published maps and institutional affiliations.